DOI: 10.1002/ejic.201100944

A Series of 3D Rare-Earth-Metal–Organic Frameworks with Isolated Guest Keggin Silicotungstate Fragments as Anion Templates

Suzhi Li,[a,b] Dongdi Zhang,[a] Yuanyuan Guo,[a] Pengtao Ma,[a] Junwei Zhao,[a] Jingping Wang,*[a] and Jingyang Niu*[a]

Keywords: Silicotungstate / Polyoxometalates / Photoluminescence / Metal–organic frameworks / Rare earths

Six rare-earth (RE) metal constructed 3D metal–organic frameworks, $[RE(pydc)(H_2O)_n]_4[SiW_{12}O_{40}]\cdot 4H_2O$ [RE = Tm^{III} (**1**), Y^{III} (**2**), Pr^{III} (**3**), La^{III} (**4**), Sm^{III} (**5**), Eu^{III} (**6**); n = 3 (**1**, **2**), 4 (**3**–**6**); H_2pydc = pyridine-2,6-dicarboxylic acid], have been synthesized and characterized by elemental analyses, inductively coupled plasma techniques, IR and UV spectroscopy, thermogravimetric analyses (for **1** and **3**), X-ray powder diffraction, and single-crystal X-ray diffraction. The structural analyses indicate that **1**–**6** are basically isostructural and show a rare host 3D framework that contains $[SiW_{12}O_{40}]^{4-}$ Keggin polyoxoanions as templates. Photoluminescence measurements reveal that **1**–**5** show the luminescence of pydc ligands, whereas **6** displays a unique red luminescence.

Introduction

Metal–organic frameworks (MOFs) have attracted much attention in recent years.[1] This is because MOFs are ideal candidates for performing coordination chemistry in extended structures because of their highly ordered nature and the flexibility with which the organic linkers can be modified,[2] and they show great promise for a number of applications, which include nonlinear optics,[3] gas storage,[4] catalysis,[5] chemical sensing,[6] biomedical imaging,[7] and drug delivery.[8]

Polyoxometalates (POMs), which are nanosized, discrete metal–oxygen cluster anions and attractive inorganic building blocks for nanostructured materials, can act as effective templates to fill some of the pores of MOFs and prevent polymers from self-interpenetrating.[9] As the search for functional MOFs continues, more attention has been steered towards synthesizing POM-based MOFs,[10–12] of which 3D POM-based MOFs have attracted considerable attention because of their enormous structural diversity and topological beauty.[10a,10b,12] In 1999, Zubieta et al. reported the first isopolymolybdate-based MOF,[12a] which possesses a 3D $[\{Fe(tetrapyridylporphyrin)\}_3Fe]_n^{4n+}$ host framework with encapsulated, isolated guest $\{Mo_6O_{19}\}^{2-}$ anions. Seven years later, Wang et al. discovered another isopolymolybdate-based MOF, $[Cu^{II}(1,10\text{-phenanthroline})_2Mo_8O_{26}]_n^{2n-}$,[10a] which was the first example of a 1D organic–inorganic hybrid POM chain and functioned as a new anionic template for the construction of a 3D framework. Keller et al. have described a 3D Keggin-type, POM-templated MOF, $[Cu_3(4,4'\text{-bipyridine})_5(MeCN)_2]PW_{12}O_{40}\cdot 2C_6H_5CN$,[12b] and some other Keggin-type, POM-supported MOFs.[10b,12c–12f] In 2008, two Dawson-type, POM-based MOFs were characterized by Liu and Su,[12g] both of which exhibit 3D host frameworks constructed from oxalate-bridged dinuclear superoctahedral secondary building units and bipyridine linkers with the voids occupied by $[P_2W_{18}O_{62}]^{6-}$ Dawson templates. Among the reported porous POM-based MOFs, most of them are transition metal (TM) constructed 3D frameworks, and reports of RE-metal-constructed 3D MOFs are very rare.[10b,13]

In comparison with 3d TM cations, RE cations, with their unique properties, such as large radii, high and variable coordination numbers, and flexible coordination geometry, can provide unique opportunities to discover new complexes with unexpected structures and properties. On the other hand, for RE-based complexes, it is well known that they exhibit excellent photophysical properties, which can contribute to f–f transitions with an extremely narrow bandwidth.[14] In recent years, a great number of 3D RE-based MOFs have been reported.[15] In their synthesis, the judicious choice of the organic linker plays a key role in the structural assembly. Previous studies have proved that different carboxylic acid ligands, such as aromatic acids,[15a] aliphatic acids,[15b] and heterocyclic acids, are good choices for the construction of these MOFs.[15c]

In our work, we employed pyridine-2,6-dicarboxylate (pydc) and Keggin-type polyoxoanions as the multifunctional ligand and anionic template, respectively. Their selec-

[a] Institute of Molecular and Crystal Engineering, College of Chemistry and Chemical Engineering, Henan University, Kaifeng, Henan 475004, P. R. China
Fax: +86-378-3886876
E-mail: jpwang@henu.edu.cn
jyniu@henu.edu.cn
[b] Department of Chemistry, Shangqiu Normal University, Shangqiu, Henan 476000, P. R. China
Supporting information for this article is available on the WWW under http://dx.doi.org/10.1002/ejic.201100944.

tion was based on the following considerations: (1) H_2pydc can be deprotonated to Hpydc$^-$ and pydc^{2-}, which provides more coordination modes; (2) the flexible and multifunctional coordination sites of H_2pydc can generate multidimensional structures; (3) the Keggin anions have comparable sizes and can act as templates for creating the porous structures of MOFs; and (4) the Keggin anions can be present as charge-compensating counterions. By allowing H_2pydc to react with the corresponding RE^{III} cations and the Keggin polyoxoanion template according to a traditional aqueous solution method, we obtained a series of RE-based, POM-templated host–guest compounds **1**–**6**. Compounds **1**–**6** are basically isostructural, and all have *I*4(1)/*a* space groups. It is interesting that they all exhibit unique porous 3D MOFs, in which the nanosized channels are occupied by Keggin polyoxoanions.

Results and Discussion

Synthesis

The rational synthesis of the desired compounds by stepwise, predesigned routes has been used extensively in synthetic chemistry. However, the synthesis of RE-based, POM-templated host–guest materials is still a great challenge, because the reaction conditions, such as temperature, pH, stoichiometry, reaction time, medium, and template identity, can have considerable influence on the outcome.[9] Compounds **1**–**6** were synthesized successfully by the reaction of the three components: $K_4[SiW_{12}O_{40}]\cdot nH_2O$, H_2pydc, and a source of the RE ions [thulium(III), yttrium(III), praseodymium(III), lanthanum(III), samarium(III), and europium(III)] in an aqueous acidic medium. The isolated yields for **1**–**6** are 30–55%, which indicates that the formation of the RE-based, POM-templated MOFs is strongly favored in a heated aqueous acidic medium. In fact, most 3D POM-templated MOFs have been synthesized under hydrothermal methods, because nucleophilic polyoxoanions are liable to form precipitates rather than crystals when they react with oxyphilic RE^{III} ions under ambient conditions.[9] In this work, we developed a traditional aqueous solution method to prepare these species. Compared with similar structures that have been recently reported – e.g. $[\{Ln(H_2O)_4(pydc)\}_4][XMo_{12}O_{40}]\cdot 2H_2O$ (Ln = La, Ce, Nd; X = Si, Ge),[13a] which was synthesized under hydrothemal conditions – our rational one-pot synthetic strategy shortened the preparation process. In order to reduce the formation of precipitates, the adjustment of the pH value of the reaction system was crucial for the crystallization of **1**–**6**. When RE nitrates were used to prepare **1**, **2**, and **4**, the pH values of the solutions were adjusted to 2.5 with an HAc/NaAc buffer solution. However, RE acetates were adopted for the syntheses of **3**, **5**, and **6**, and the pH values of the solutions were adjusted to 4.0 with HAc. Parallel experiments showed that crystals of **1**–**6** were only obtained in high yields in the pH range 2.5–4.0.

Structural Description

Structural analysis shows that **1**–**6** all crystallize in the tetragonal *I*4(1)/*a* space group, and their molecular structures all comprise a noncoordinating polyoxoanion $[SiW_{12}O_{40}]^{4-}$, four RE coordination cations $[RE(pydc)(H_2O)_n]^+$ [n = 3 (**1**, **2**), 4 (**3**–**6**)], and four water molecules of crystallization (Figure 1a). In **1**–**6**, $[SiW_{12}O_{40}]^{4-}$ exhibits a classical Keggin-type structure, in which the central SiO_4 tetrahedron is surrounded by twelve WO_6 octahedra arranged in four groups of three edge-sharing W_3O_{13} octahedral subunits. Each trinuclear W_3O_{13} subunit is in turn linked by a corner so that they share the central SiO_4 tetrahedron (Figure 1b).

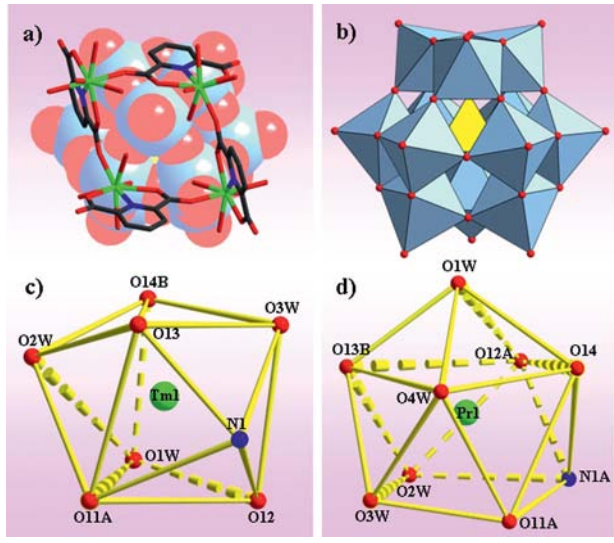

Figure 1. (a) Space-filling and stick representation of the structural unit of **1**–**6**. Water molecules of crystallization and hydrogen atoms are omitted for clarity. (b) Polyhedral representation of $[SiW_{12}O_{40}]^{4-}$ in **1**–**6**. (c) Bicapped triangular-prismatic geometry of $Tm(1)^{3+}$ in **1** (symmetry transformation: A = 0.25 – x, 0.25 + y, 0.25 + z; B = 0.25 – x, –0.25 + y, 0.25 – z). (d) Monocapped square-antiprismatic coordination geometry of $Pr(1)^{3+}$ in **3** (symmetry transformation: A = –0.25 + x, 1.25 – y, –0.25 + z; B = –0.5 + x, y, –0.5 – z).

Compounds **1**–**6** are basically isostructural, the only difference is that the RE cations in **1** and **2** have different coordination environments to those in **3**–**6**. As examples, only the structures of **1** and **3** are described in detail. The structural unit of **1** consists of a polyoxoanion $[SiW_{12}O_{40}]^{4-}$, four $[Tm(pydc)(H_2O)_3]^+$ coordination cations, and four water molecules of crystallization. In **1**, $Tm(1)^{3+}$ is in a distorted, bicapped trigonal-prismatic geometry (Figure 1c), which is defined by four carboxyl oxygen atoms from three pydc ligands [Tm(1)–O 2.305(8)–2.414(7) Å], a nitrogen atom from a pydc ligand [Tm(1)–N 2.442(8) Å], and three terminal water ligands [Tm(1)–O 2.319(8)–2.351(7) Å]. In the coordination configuration of $Tm(1)^{3+}$, the O13, O14B, and O3W group and the O11A, O12, and O1W group constitute the two bottom planes of the trigonal prism with the dihedral angle between the two bottom surfaces of 7.8°, and the distances between Tm(1) and the two bottom planes are

1.6352 and 1.3884 Å, respectively. The O13, O11A, O1W, and O14B group, the O13, O11A, O12, and O3W group, and the O3W, O12, O1W, and O14B group form the three side planes of the trigonal prism, and their average deviations are 0.1434, 0.1997, and 0.0340 Å, respectively. The distances between Tm(1) and the three side planes are 0.6326, 0.7781, and 1.2500 Å, respectively. Interestingly, O2W and N1 occupy the two capping positions that cover the side planes defined by the O13, O11A, O1W, and O14B group and the O13, O11A, O12, and O3W group, respectively. The distances between the two caps and the side planes are 1.7091 and 1.6628 Å, respectively. The structural unit of **3** consists of an $[SiW_{12}O_{40}]^{4-}$ polyoxoanion, four $[Pr(pydc)(H_2O)_4]^+$ coordination cations, and four water molecules of crystallization. In **3**, $Pr(1)^{3+}$ is nine-coordinate and adopts a distorted, monocapped square-antiprismatic geometry (Figure 1d). $Pr(1)^{3+}$ bonds to four carboxyl oxygen atoms from three pydc ligands [Pr(1)–O 2.479(7)–2.509(7) Å], a nitrogen atom from a pydc ligand [Pr(1)–N 2.615(7) Å], and four terminal water molecules [Pr(1)–O 2.510(7)–2.666(10) Å]. In the coordination polyhedron around $Pr(1)^{3+}$, the O4W, O14, O12A, and O13B group and the O11A, N1A, O2W and O3W group define the two bottom planes of the square antiprism with average deviations of 0.0980 and 0.1206 Å, respectively. The dihedral angle between the two bottom surfaces is 8.5°. O1W is in the capping position, and the distance between O1W and the two bottom planes are 1.6886 and 4.0432 Å, respectively. The distances between Pr(1) and the two bottom planes are 0.8156 and 1.5890 Å, respectively. These data indicate that the bicapped trigonal-prismatic geometry of Tm^{3+} in **1** and the square-antiprismatic geometry of Pr^{3+} in **3** are severely distorted. The difference in the coordination number between the Tm^{3+} and Pr^{3+} cations is a direct consequence of the lanthanide contraction, which is often observed.[16]

The most interesting feature of these complexes is that each pydc acts as a pentadentate ligand and contributes four oxygen atoms and a nitrogen atom that combine with three RE cations [RE = Tm^{3+} (**1**), Pr^{3+} (**3**)]. Four $[RE(pydc)(H_2O)_n]^+$ units [n = 3 (**1**), 4 (**3**)] connect to each other by sharing eight carboxylic oxygen atoms from four pydc ligands to form a four-membered ring (Figure 1a). The Tm···Tm distances vary from 6.2225(10) to 6.3033(8) Å for **1**, and the Pr···Pr distances are in the range of 6.4219(10)–6.4638(9) Å for **3**. These tetracylic rings intersect each other to form an intriguing 3D MOF, in which RE ions interconnect to form numerous rectangular and square four-membered ring channels in the *ab* plane and alternate four- and eight-membered ring channels in the *ac* plane. In the 3D MOF, the square four-membered ring channels in the *ab* plane and the eight-membered ring channels in the *ac* plane are filled by the guest $[SiW_{12}O_{40}]^{4-}$ Keggin polyoxoanions (Figure 2a and b). When the $[RE(pydc)(H_2O)_n]^+$ coordination cation is viewed as a four-connected node, the 3D MOF can be simplified to a (4,4)-connected 3D topological structure with Schläfli symbol ($4^3{\cdot}6^2{\cdot}8$) (Figure 2c and d), in which each $[RE(pydc)(H_2O)_n]^+$ coordination cation connects to four neighbors.

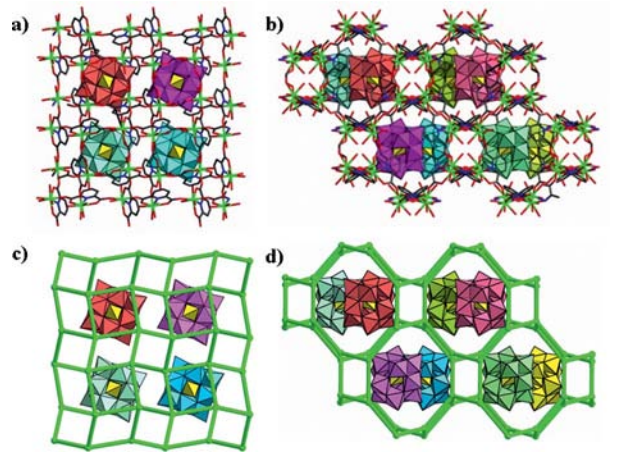

Figure 2. (a) View of the 3D framework of RE coordination cations in the *ab* plane. (b) View of the (4,4)-connected 3D topological structure of RE coordination cations in the *ab* plane. (c) View of the (4,4)-connected 3D topological structure of **1**–**6** in the *ab* plane.

X-ray Powder Diffraction (XRPD)

The experimental XRPD patterns of the bulk products of **1**–**6** are in good agreement with the simulated patterns that are based on the results from single-crystal XRD, which indicates the phase purity of the samples (Figure 3). The different intensities of the experimental and simulated XRPD patterns are due to the variation in the preferred orientation of the powder sample during data collection.

IR Spectroscopy

The peak shapes in the IR spectra (400–1600 cm^{-1}) of **1**–**6** are similar (Figure S1a), which indicates that the structures of **1**–**6** are almost the same. This is in good agreement with the results of the single-crystal XRD structural analysis. In the low-wavenumber region ($\tilde{\nu} < 1000\ cm^{-1}$), characteristic vibration patterns derived from the Keggin frameworks are observed.[5c] Four characteristic bands are assigned to $\nu(W–O_t)$, $\nu(Si–O_a)$, $\nu(W–O_b)$, and $\nu(W–O_c)$, which appear at 966, 918, 883 and 761, 802 cm^{-1} for **1**, 967, 917, 887 and 760, 801 cm^{-1} for **2**, 968, 917, 883 and 761, 802 cm^{-1} for **3**, 970, 923, 881 and 762, 807 cm^{-1} for **4**, 969, 916, 883 and 757, 801 cm^{-1} for **5**, and 969, 920, 886 and 761, 805 cm^{-1} for **6**. In comparison with the IR spectrum of the $K_4[SiW_{12}O_{40}]{\cdot}nH_2O$ precursor (Figure S1b), the $\nu(W–O_t)$ vibration frequencies for **1**–**6** are redshifted by 9–13 cm^{-1}. The most likely reason for this is that the RE metal complexes have stronger interactions with the terminal oxygen atoms of the polyoxoanions, which impairs the $W–O_t$ bond, reduces the $W–O_t$ bond force constant, and leads to the decrease of the $W–O_t$ vibration frequency. The $\nu(W–O_c)$ vibrational band for **1**–**6** is split into two peaks, possibly because the polyoxoanionic symmetry of **1**–**6** is decreased compared to that of $K_4[SiW_{12}O_{40}]{\cdot}nH_2O$. In addition, the resonances at 1382–1455 cm^{-1} and 1570–1615 cm^{-1} in **1**–**6** are assigned to the symmetric stretching vibration and asymmetric stretching vibration of the carboxylate groups.

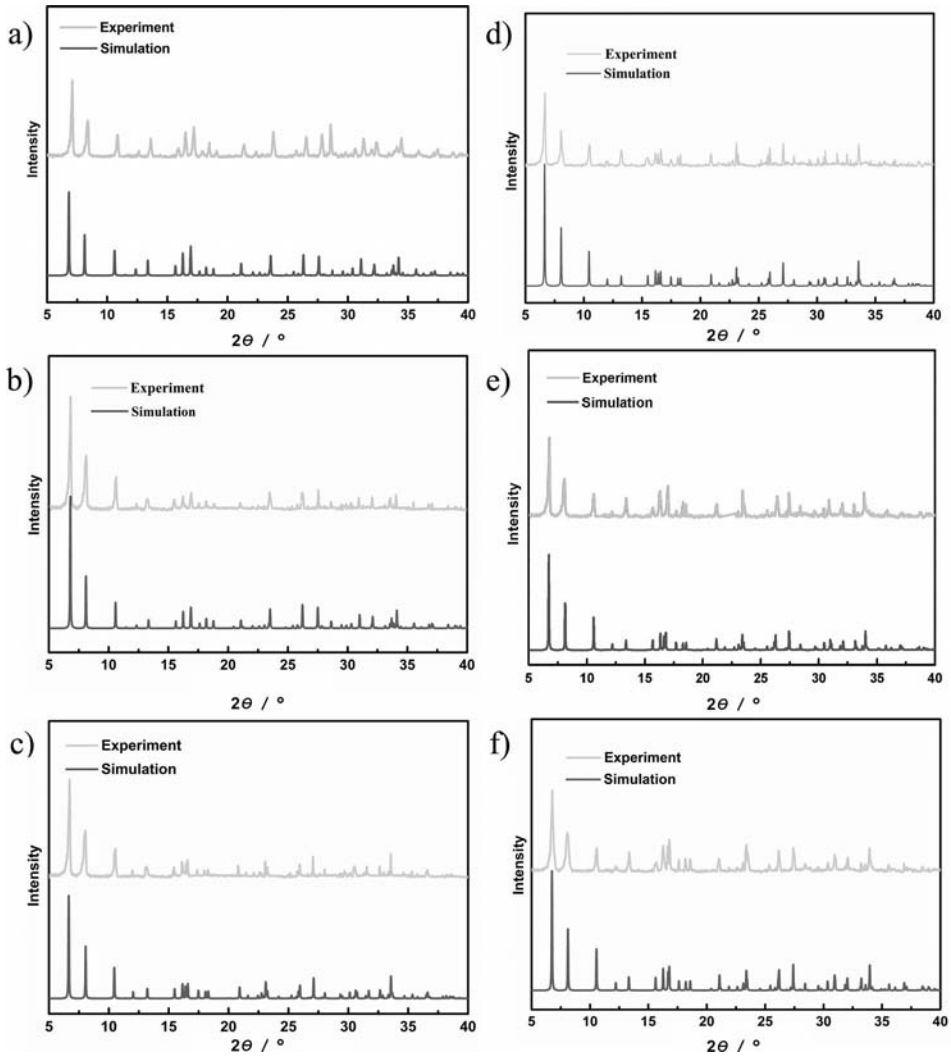

Figure 3. Comparison of the simulated and experimental XRPD patterns of **1** (a), **2** (b), **3** (c), **4** (d), **5** (e), and **6** (f).

UV Spectroscopy

The UV spectra (Figure S2) of **1**, **3**, and **5** in aqueous solution display a strong absorption peak at ca. 270 nm and a weak peak at 280 nm. The stronger absorption is assigned to the charge-transfer transition of the $O_{b,c}\rightarrow W$ bands, which suggests the presence of the Keggin polyoxoanions. In addition, compared with the UV spectrum of the free ligand, the weaker absorption at ca. 280 nm can be ascribed to a metal-to-ligand charge transfer (MLCT).

Photoluminescent Properties

The solid-state photoluminescent properties of **1**–**6** were measured at room temperature. When **1**–**5** were excited at 401, 391, 388, 396, and 384 nm, respectively, they all exhibited two similar emission peaks at about 501, 595; 505, 586; 502, 584; 509, 590; and 498, 575 nm, respectively (Figure 4a). In order to understand the nature of the emission bands, the photoluminescent properties of free H_2pydc were also studied, the emission peaks of which are located at 424 and 569 nm (Figure 4b). However, when pydc was coordinated by RE^{3+}, the emission bands redshifted to different extents. According to previous reports, the emission bands of **1**–**5** may be assigned to MLCT.[17] When Eu^{III}-based **6** was excited at 395 nm, it displays an intense red luminescence and exhibits characteristic luminescent bands at 581, 594, 615, 652, and 702 nm (Figure 4c), which correspond to the transitions from the $^5D_0$ state to the ^7F_J (J = 0–4) levels, respectively.[13c,18] Lanthanide luminescence is very sensitive to the local environment around the lanthanide center.[19] The appearance of the symmetry-forbidden $^5D_0\rightarrow{}^7F_0$ emission at 581 nm indicates that the Eu^{3+} cations in **6** occupy sites with low symmetry and no inversion center,[18e,18f,20] which is further confirmed by the fact that the $^5D_0\rightarrow{}^7F_2$ transition is much more intense than the $^5D_0\rightarrow{}^7F_1$ transi-

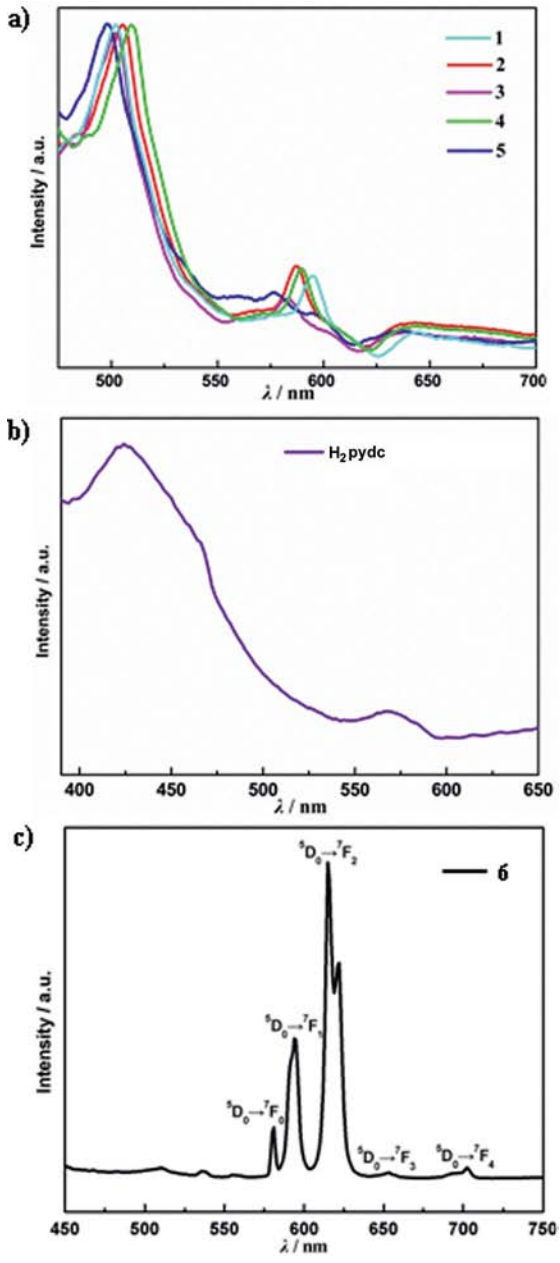

Figure 4. Solid-state emission spectra of **1**–**6** and H_2pydc at room temperature.

tion. This is consistent with the results of the single-crystal XRD analysis, which showed that the Eu^{3+} cations have a distorted, monocapped square-antiprismatic geometry.

Thermogravimetric (TG) Analysis

Compounds **1**–**6** are basically isostructural, so only the thermal properties of **1** and **3** (Figure S3) were measured in an air flow with a heating rate of 10 °C min^{-1} from 25 to 800 °C. The TG curve of **1** indicates two weight-loss steps, which are associated with the loss of lattice water molecules, coordination water molecules, and pydc ligands with a total loss of 20.56% (calcd. 21.09%). The first weight loss of 6.35% between 25 and 274 °C corresponds to the loss of four lattice water molecules and twelve coordination water molecules (calcd. 6.41%). One endothermic peak is observed at 137.0 °C in the corresponding differential thermal analysis (DTA) curve. On further heating, the materials lose weight continuously during the second step with a combined weight loss of 14.21% from 274 to 800 °C, which corresponds to the decomposition of four pydc ligands (calcd. 14.68%). In the corresponding DTA curve, one obvious exothermic peak at 624.5 °C and several small exothermic peaks are observed, which arise from the combustion of pydc ligands and polyoxoanion skeletons. The TG curve of **3** is similar to that of **1**; the weight loss of 7.74% during the first step from 25 to 293 °C involves the loss of four lattice water molecules and 16 coordinated water molecules (calcd. 8.08%). The second step, with a weight loss of 14.08% from 293 to 800 °C, corresponds to the removal of four pydc ligands (calcd. 14.81%). These analyses reveal that the experimental values are approximately consistent with the theoretical values.

To investigate the decomposition process of the compounds with increasing temperature, variable-temperature IR spectra of **1** were measured. As shown in Figure 5a, the IR spectra show no obvious change in the temperature range of 100–400 °C. When the temperature increased to 500 °C, the characteristic pydc bands and the four charac-

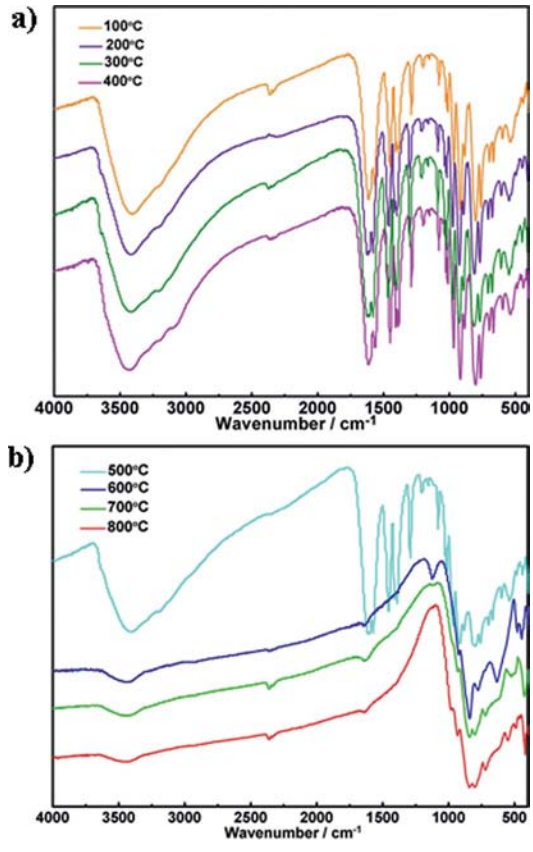

Figure 5. (a) Variable-temperature IR spectra of **1** at 100, 200, 300, and 400 °C. (b) Variable-temperature IR spectra of **1** at 500, 600, 700, and 800 °C.

teristic bands of the heteropolyanions are still observed but with weaker intensities (Figure 5b). When the temperature increased to 600 °C, the characteristic pydc bands became undetectable, and the characteristic ν(W–O_t), ν(Si–O_a), ν(W–O_b), and ν(W–O_c) vibrations vanished completely. This shows that the skeleton of **1** decomposes at ca. 600 °C, which is in accordance with the result of the TG analysis.

Conclusions

Six RE-metal-constructed 3D MOFs, $[RE(pydc)(H_2O)_n]_4[SiW_{12}O_{40}]\cdot 4H_2O$, have been successfully synthesized by a traditional aqueous solution method. Structural analyses indicate that **1**–**6** are basically isostructural and show a rare 3D framework that contains polyoxoanions as anionic templates. The photoluminescence measurements reveal that **6** shows obvious red luminescence. We are currently investigating if other Keggin polyoxoanions can form analogues of **1**–**6**, and we will also study the reactivities of analogues of the carboxylic acid ligands with different Keggin polyoxoanions.

Experimental Section

General Methods and Materials: All reagents were used as purchased without further purification. Elemental analysis (C, H, and N) was performed with a Perkin–Elmer 240C elemental analyzer. Inductively coupled plasma analysis was performed with a Perkin–Elmer Optima 2000 ICP-OES spectrometer. IR spectra were obtained from a solid sample palletized with KBr with a Nicolet 170 SXFT-IR spectrometer in the range 400–4000 cm^{-1}. UV absorption spectra were obtained with a U-4100 spectrometer at room temperature. TG analysis was performed in N_2 with a Perkin–Elmer 7 instrument. XRPD measurements were performed with a Philips X'Pert-MPD instrument with Cu-K_α radiation (λ = 1.54056 Å) in the angular range 2θ = 10–40° at 293 K. Fluorescence spectra were measured with a HITACHI F-7000 Fluorescence spectrophotometer.

$[Tm(pydc)(H_2O)_3]_4[SiW_{12}O_{40}]\cdot 4H_2O$ (1): An aqueous solution (20 mL) that contained $K_4[\alpha\text{-}SiW_{12}O_{40}]\cdot nH_2O$ (0.85 g) was added to a CH_3CH_2OH/H_2O (20 mL, 1:1, volume ratio) solution that contained H_2pydc (0.10 g, 0.60 mmol) and $Tm(NO_3)_3\cdot 6H_2O$ (0.50 g, 1.08 mmol). The pH was adjusted to 2.5 with HAc/NaAc buffer solution (pH = 4.5). The resulting mixture was heated in a water bath (80 °C) for 1 h and filtered after cooling. Slow concentration at room temperature led to the formation of colorless crystals suitable for XRD within 2–3 weeks, which were collected by filtration and dried in air (yield ca. 40% based on $K_4[\alpha\text{-}SiW_{12}O_{40}]\cdot nH_2O$). $C_{28}H_{44}N_4O_{72}SiTm_4W_{12}$ (4498.66): calcd. C 7.48, H 0.99, N 1.25, Si 0.62, Tm 15.02, W 49.04; found C 7.41, H 1.08, N 1.16, Si 0.67, Tm 15.10, W 48.98. IR (KBr; Figure S1a, Table S1): $\tilde{\nu}$ = 1610 (s), 1571 (s), 1450 (s), 1389 (s), 1292 (s), 1199 (m), 1150 (w), 1081 (m), 1012 (s), 966 (s), 918 (s), 883 (w), 802 (s), 761 (s), 696 (m), 665 (m), 593 (w), 538 (m) cm^{-1}.

$[Y(pydc)(H_2O)_3]_4[SiW_{12}O_{40}]\cdot 4H_2O$ (2): The preparation of **2** was similar to that of **1**, except that $Y(NO_3)_3\cdot 6H_2O$ (0.50 g, 1.31 mmol) replaced $Tm(NO_3)_3\cdot 6H_2O$. Slow concentration at room temperature afforded colorless crystals suitable for XRD after 1–2 weeks, which were collected by filtration and dried in air (yield ca. 45% based on $K_4[\alpha\text{-}SiW_{12}O_{40}]\cdot nH_2O$). $C_{28}H_{44}N_4O_{72}SiW_{12}Y_4$ (4178.55): calcd. C 8.05, H 1.06, N 1.34, Si 0.67, Y 8.51, W 52.80; found C 8.15, H 1.24, N 1.25, Si 0.71, Y 8.44, W 52.87. IR (KBr; Figure S1a, Table S1): $\tilde{\nu}$ = 1614 (s), 1571 (s), 1450 (s), 1392 (s), 1292 (s), 1201 (m), 1152 (w), 1081 (m), 1013 (s), 967 (s), 917 (s), 887 (w), 801 (s), 760 (s), 698 (m), 665 (m), 594 (w), 538 (m) cm^{-1}.

$[Pr(pydc)(H_2O)_4]_4[SiW_{12}O_{40}]\cdot 4H_2O$ (3): The preparation of **3** was similar to that of **1**, except that $Pr(CH_3COO)_3\cdot 6H_2O$ (0.50 g, 1.17 mmol) replaced $Tm(NO_3)_3\cdot 6H_2O$. In addition, the pH of the resulting solution was adjusted to 4.0 with HAc. Slow concentration at room temperature afforded green crystals suitable for XRD after 1 week, which were collected by filtration and dried in air (yield ca. 55% based on $K_4[\alpha\text{-}SiW_{12}O_{40}]\cdot nH_2O$). $C_{28}H_{52}N_4O_{76}Pr_4SiW_{12}$ (4458.62): calcd. C 7.54, H 1.18, N 1.26, Si 0.63, Pr 12.64, W 49.48; found C 7.42, H 1.29, N 1.20, Si 0.69, Pr 12.57, W 49.41. IR (KBr; Figure S1a, Table S1): $\tilde{\nu}$ = 1607 (s), 1570 (s), 1450 (s), 1382 (s), 1283 (s), 1201 (m), 1150 (w), 1081 (m), 1014 (s), 968 (s), 917 (s), 883 (w), 802 (s), 761 (s), 699 (m), 663 (m), 590 (w), 536 (m) cm^{-1}.

$[La(pydc)(H_2O)_4]_4[SiW_{12}O_{40}]\cdot 4H_2O$ (4): The preparation of **4** was similar to that of **1**, except that $La(NO_3)_3\cdot 6H_2O$ (0.50 g, 1.15 mmol) replaced $Tm(NO_3)_3\cdot 6H_2O$. Slow concentration at room temperature afforded colorless crystals suitable for XRD after 2–3 weeks, which were collected by filtration and dried in air (yield ca. 30% based on $K_4[\alpha\text{-}SiW_{12}O_{40}]\cdot nH_2O$). $C_{28}H_{52}La_4N_4O_{76}SiW_{12}$ (4450.61): calcd. C 7.56, H 1.18, N 1.26, Si 0.63, La 12.48, W 49.57; found C 7.48, H 1.29, N 1.11, Si 0.69, La 12.40, W 49.68. IR (KBr; Figure S1a, Table S1): $\tilde{\nu}$ = 1615 (s), 1572 (s), 1455 (s), 1390 (s), 1292 (s), 1198 (m), 1152 (w), 1080 (m), 1017 (s), 970 (s), 923 (s), 879 (w), 807 (s), 762 (s), 705 (m), 668 (m), 598 (w), 542 (m) cm^{-1}.

$[Sm(pydc)(H_2O)_4]_4[SiW_{12}O_{40}]\cdot 4H_2O$ (5): The preparation of **5** was similar to that of **3**, except that $Sm(CH_3COO)_3\cdot 6H_2O$ (0.50 g, 1.15 mmol) replaced $Pr(CH_3COO)_3\cdot 6H_2O$. Slow concentration at room temperature afforded yellow crystals suitable for XRD after 2–3 weeks, which were collected by filtration and dried in air (yield ca. 50% based on $K_4[\alpha\text{-}SiW_{12}O_{40}]\cdot nH_2O$). $C_{28}H_{52}N_4O_{76}SiSm_4W_{12}$ (4496.59): calcd. C 7.48, H 1.17, N 1.25, Si 0.62, Sm 13.38, W 49.06; found C 7.39, H 1.29, N 1.17, Si 0.69, Sm 13.46, W 49.00. IR (KBr; Figure S1a, Table S1): $\tilde{\nu}$ = 1612 (s), 1571 (s), 1449 (s), 1386 (s), 1288 (s), 1201 (m), 1150 (w), 1079 (m), 1009 (s), 969 (s), 916 (s), 883 (w), 801 (s), 757 (s), 695 (m), 665 (m), 591 (w), 539 (m) cm^{-1}.

$[Eu(pydc)(H_2O)_4]_4[SiW_{12}O_{40}]\cdot 4H_2O$ (6): The preparation of **6** was similar to that of **3**, except that $Eu(CH_3COO)_3\cdot 6H_2O$ (0.50 g, 1.14 mmol) replaced $Pr(CH_3COO)_3\cdot 6H_2O$. Slow concentration at room temperature afforded colorless crystals suitable for XRD after 2–3 weeks, which were collected by filtration and dried in air (yield ca. 45% based on $K_4[\alpha\text{-}SiW_{12}O_{40}]\cdot nH_2O$). $C_{28}H_{52}Eu_4N_4O_{76}SiW_{12}$ (4502.83): calcd. C 7.45, H 1.16, N 1.24, Si 0.62, Eu 13.50, W 48.99; found C 7.34, H 1.29, N 1.18, Si 0.68, Eu 13.43, W 48.91. IR (KBr; Figure S1a, Table S1): $\tilde{\nu}$ = 1612 (s), 1571 (s), 1449 (s), 1390 (s), 1290 (s), 1201 (m), 1150 (w), 1079 (m), 1013 (s), 969 (s), 920 (s), 886 (w), 805 (s), 761 (s), 699 (m), 665 (m), 595 (w), 539 (m) cm^{-1}.

X-ray Crystallography: Intensity data for **1**–**6** were collected with a Bruker CCD Apex-II diffractometer with Mo-K_α radiation (λ = 0.71073 Å) at 296 K. The structures of **1**–**6** were resolved by direct methods using the SHELXTL-97 program package.[21] The remaining atoms were found from successive full-matrix least-squares refinements on F^2 and Fourier syntheses. Lorentz polarization and multiscan absorption corrections were applied. Hydrogen atoms associated with the water molecules were not located from the differ-

Table 1. Crystallographic data and structural refinement for **1**–**6**.

	1	**2**	**3**	**4**	**5**	**6**
Empirical formula	$C_{28}H_{44}N_4O_{72}SiW_{12}Tm_4$	$C_{28}H_{44}N_4O_{72}SiW_{12}Y_4$	$C_{28}H_{52}N_4O_{76}SiW_{12}Pr_4$	$C_{28}H_{52}N_4O_{76}SiW_{12}La_4$	$C_{28}H_{52}N_4O_{76}SiW_{12}Sm_4$	$C_{28}H_{52}N_4O_{76}SiW_{12}Eu_4$
Formula mass	4498.54	4178.42	4458.49	4450.48	4496.30	4502.72
Temperature [K]	296(2)	296(2)	296(2)	296(2)	296(2)	296(2)
Crystal system	tetragonal	tetragonal	tetragonal	tetragonal	tetragonal	tetragonal
Space group	*I*4(1)/*a*	*I*4(1)/*a*	*I*4(1)/*a*	*I*4(1)/*a*	*I*4(1)/*a*	*I*4(1)/*a*
a [Å]	21.751(3)	21.8154(9)	21.9314(10)	21.9285(8)	21.685(5)	21.7777(7)
b [Å]	21.751(3)	21.8154(9)	21.9314(10)	21.9285(8)	21.685(5)	21.7777(7)
c [Å]	16.1438(15)	16.1967(12)	16.7059(15)	16.7265(12)	16.470(7)	16.4167(10)
V [Å^3]	7637.7(17)	7708.2(7)	8035.3(9)	8043.1(7)	7745(4)	7785.9(6)
Z	4	4	4	4	4	4
F (000)	7848	7496	7816	7784	7864	7880
$\rho_{calcd.}$ [g cm^{-3}]	3.884	3.601	3.652	3.642	3.822	3.807
μ [mm^{-1}]	22.722	20.938	19.613	19.295	20.864	20.960
Reflections collected	19092	19619	22656	38747	18340	20721
Independent reflections	3353	3567	3531	3532	3406	3613
GOOF	0.999	1.055	1.061	1.048	1.053	1.062
R(int)	0.1417	0.0643	0.0478	0.0548	0.0475	0.0427
Final *R* indices [$I = 2\sigma(I)$]	$R_1 = 0.0320$ $\omega R_2 = 0.0700$	$R_1 = 0.0489$ $\omega R_2 = 0.1232$	$R_1 = 0.0309$ $\omega R_2 = 0.0669$	$R_1 = 0.0247$ $\omega R_2 = 0.0521$	$R_1 = 0.0311$ $\omega R_2 = 0.0726$	$R_1 = 0.0300$ $\omega R_2 = 0.0714$
R indices (all data)	$R_1 = 0.0515$ $\omega R_2 = 0.0761$	$R_1 = 0.0681$ $\omega R_2 = 0.1318$	$R_1 = 0.0412$ $\omega R_2 = 0.0706$	$R_1 = 0.0327$ $\omega R_2 = 0.0542$	$R_1 = 0.0479$ $\omega R_2 = 0.0779$	$R_1 = 0.0402$ $\omega R_2 = 0.0751$

ence Fourier map. Positions of the hydrogen atoms attached to the carbon atoms were geometrically placed. All hydrogen atoms were refined isotropically as a riding mode by using the default SHELXTL parameters. Crystallographic data and structural refinements for **1**–**6** are summarized in Table 1. CCDC-808295 (for **1**), -808296 (for **2**), -808297 (for **3**), -808298 (for **4**), -808299 (for **5**), and -808300 (for **6**) contain the supplementary crystallographic data for this paper. These data can be obtained free of charge from The Cambridge Crystallographic Data Centre via www.ccdc.cam.ac.uk/data_request/cif.

Supporting Information (see footnote on the first page of this article): IR and UV spectra, TG/DTA curves, IR data.

Acknowledgments

This work was supported by the National Natural Science Foundation of China, the Special Research Fund for the Doctoral Program of Higher Education, the Innovation Scientists and Technicians Troop Construction Projects of Henan Province, the Foundation of Education Department of Henan Province, and the Natural Science Foundation of Henan Province.

[1] a) J. M. Thomas, *Angew. Chem.* **1999**, *111*, 3800; *Angew. Chem. Int. Ed.* **1999**, *38*, 3588–3628; b) K. Biradha, Y. Hongo, M. Fujita, *Angew. Chem.* **2000**, *112*, 4001; *Angew. Chem. Int. Ed.* **2000**, *39*, 3843–3845; c) B. Moulton, M. J. Zaworotko, *Chem. Rev.* **2001**, *101*, 1629–1658; d) H. L. Li, M. Eddaoudi, M. O'Keeffe, O. M. Yaghi, *Nature* **1999**, *402*, 276–279; e) S. Kitagawa, R. Kitaura, S. Noro, *Angew. Chem.* **2004**, *116*, 2388; *Angew. Chem. Int. Ed.* **2004**, *43*, 2334–2375; f) M. Eddaoudi, D. B. Moler, H. L. Li, B. L. Chen, T. M. Reineke, M. O'Keeffe, O. M. Yaghi, *Acc. Chem. Res.* **2001**, *34*, 319–330; g) U. Kortz, S. S. Hamzeh, N. A. Nasser, *Chem. Eur. J.* **2003**, *9*, 2945–2952; h) Z. E. Lin, J. Zhang, J. T. Zhao, S. T. Zheng, C. Y. Pan, G. M. Wang, G. Y. Yang, *Angew. Chem.* **2005**, *117*, 7041; *Angew. Chem. Int. Ed.* **2005**, *44*, 6881–6884.

[2] C. J. Doonan, W. Morris, H. Furukawa, O. M. Yaghi, *J. Am. Chem. Soc.* **2009**, *131*, 9492–9493.

[3] a) O. R. Evans, W. Lin, *Acc. Chem. Res.* **2002**, *35*, 511–522; b) Y. Liu, G. Li, X. Li, Y. Cui, *Angew. Chem.* **2007**, *119*, 6417; *Angew. Chem. Int. Ed.* **2007**, *46*, 6301–6304.

[4] a) D. Mircea, J. R. Long, *Angew. Chem.* **2008**, *120*, 6870; *Angew. Chem. Int. Ed.* **2008**, *47*, 6766–6779; b) D. Zhao, D. Yuan, H. C. Zhou, *Energy Environ. Sci.* **2008**, *1*, 222–235; c) J. L. C. Rowsell, O. M. Yaghi, *Angew. Chem.* **2005**, *117*, 4748; *Angew. Chem. Int. Ed.* **2005**, *44*, 4670–4679; d) B. Kesanli, Y. Cui, M. Smith, E. Bittner, B. Bockrath, W. Lin, *Angew. Chem.* **2005**, *117*, 74; *Angew. Chem. Int. Ed.* **2005**, *44*, 72–75; e) B. Chen, X. Zhao, A. Putkham, K. Hong, E. B. Lobkovsky, E. J. Hurtado, A. J. Fletcher, K. M. Thomas, *J. Am. Chem. Soc.* **2008**, *130*, 6411–6423.

[5] a) C. Wu, A. Hu, L. Zhang, W. Lin, *J. Am. Chem. Soc.* **2005**, *127*, 8940–8941; b) S. H. Cho, B. Ma, S. T. Nguyen, J. T. Hupp, T. E. Albrecht-Schmitt, *Chem. Commun.* **2006**, 2563–2565; c) C. D. Wu, W. Lin, *Angew. Chem.* **2007**, *119*, 1093; *Angew. Chem. Int. Ed.* **2007**, *46*, 1075–1078.

[6] a) M. D. Allendorf, R. J. T. Houk, L. Andruszkiewicz, A. A. Talin, J. Pikarsky, A. Choudhury, K. A. Gall, P. J. Hesketh, *J. Am. Chem. Soc.* **2008**, *130*, 14404–14405; b) B. Chen, L. Wang, Y. Xiao, F. R. Fronczek, M. Xue, Y. Cui, G. Qian, *Angew. Chem.* **2009**, *121*, 508; *Angew. Chem. Int. Ed.* **2009**, *48*, 500–503.

[7] a) K. M. L. Taylor, W. J. Rieter, W. Lin, *J. Am. Chem. Soc.* **2008**, *130*, 14358–14359; b) K. M. L. Taylor, A. Jin, W. Lin, *Angew. Chem.* **2008**, *120*, 7836; *Angew. Chem. Int. Ed.* **2008**, *47*, 7722–7725.

[8] a) P. Horcajada, C. Serre, G. Maurin, N. A. Ramsahye, F. Balas, M. Vallet-Regí, M. Sebban, T. Taulelle, G. Férey, *J. Am. Chem. Soc.* **2008**, *130*, 6774–6780; b) W. J. Rieter, K. M. Pott, K. M. L. Taylor, W. Lin, *J. Am. Chem. Soc.* **2008**, *130*, 11584–11585.

[9] R. M. Yu, X. F. Kuang, X. Y. Wu, C. Z. Lu, J. P. Donahue, *Coord. Chem. Rev.* **2009**, *253*, 2872–2890.

[10] a) H. Jin, Y. Qi, E. Wang, Y. Li, C. Qin, X. Wang, S. Chang, *Eur. J. Inorg. Chem.* **2006**, 4541–4545; b) M. L. Wei, C. He, Q. Z. Sun, Q. J. Meng, C. Y. Duan, *Inorg. Chem.* **2007**, *46*, 5957–5966; c) L. San Felices, P. Vitoria, J. M. Gutierrez-Zorrilla, L. Lezama, R. S. Einoso, *Inorg. Chem.* **2006**, *45*, 7748–7757; d) J. Sha, J. Peng, A. X. Tian, H. S. Liu, J. Chen, P. P. Zhang, Z. M. Su, *Cryst. Growth Des.* **2007**, *7*, 2535–2541; e) Y. Wang, D. R. Xiao, L. F. Fan, E. B. Wang, J. Liu, *J. Mol. Struct.* **2007**, *843*, 87–94; f) L. Yuan, C. Qin, X. L. Wang, E. B. Wang, S. Chang, *Eur. J. Inorg. Chem.* **2008**, 4936–4942; g) P. Q. Zheng, Y. P. Ren, L. S. Long, R. B. Huang, L. S. Zheng, *Inorg. Chem.*

2005, *44*, 1190–1192; h) Y. Wang, D. R. Xiao, E. B. Wang, L. L. Fan, J. Liu, *Transition Met. Chem.* **2007**, *32*, 950–959; i) K. Uehara, H. Nakao, R. Kawamoto, S. Hikichi, N. Mizuno, *Inorg. Chem.* **2006**, *45*, 9448–9453; j) D. Hagrman, C. Zubieta, D. J. Rose, J. Zubieta, R. C. Haushalter, *Angew. Chem.* **1997**, *109*, 904; *Angew. Chem. Int. Ed. Engl.* **1997**, *36*, 873–876; k) X. J. Kong, Y. P. Ren, P. Q. Zheng, Y. X. Long, L. S. Long, *Inorg. Chem.* **2006**, *45*, 10702–10711; l) L. M. Zheng, Y. Wang, X. Wang, J. D. Korp, A. J. Jacobson, *Inorg. Chem.* **2001**, *40*, 1380–1385; m) L. Wang, X. P. Sun, M. L. Liu, Y. Q. Gao, W. Gu, X. Liu, *J. Cluster Sci.* **2008**, *19*, 531–542; n) Q. G. Zhai, X. Y. Wu, S. M. Chen, Z. G. Zhao, C. Z. Lu, *Inorg. Chem.* **2007**, *46*, 5046–5058; o) S. L. Li, Y. Q. Lan, J. F. Ma, J. Yang, J. Liu, Y. M. Fu, Z. M. Su, *Dalton Trans.* **2008**, 2015–2025; p) A. X. Tian, J. Ying, J. Peng, J. Q. Sha, H. J. Pang, P. P. Zhang, Y. Chen, M. Zhu, Z. M. Su, *Cryst. Growth Des.* **2008**, *8*, 3717–3724; q) A. X. Tian, J. Ying, J. Peng, J. Q. Sha, H. J. Pang, P. P. Zhang, Y. Chen, M. Zhu, Z. M. Su, *Inorg. Chem.* **2009**, *48*, 100–110; r) B. X. Dong, J. Peng, P. P. Zhang, A. X. Tian, J. Chen, B. Xue, *Inorg. Chem. Commun.* **2007**, *10*, 839–842; s) Y. Q. Lan, S. L. Li, X. L. Wang, K. Z. Shao, Z. M. Su, E. B. Wang, *Inorg. Chem.* **2008**, *47*, 529–534.

[11] a) C. Y. Sun, Y. G. Li, E. B. Wang, D. R. Xiao, H. Y. An, L. Xu, *Inorg. Chem.* **2007**, *46*, 1563–1574; b) Y. G. Li, L. M. Dai, Y. H. Wang, X. L. Wang, E. B. Wang, Z. M. Sun, L. Xu, *Chem. Commun.* **2007**, 2593–2595; c) Q. G. Zhai, X. Y. Wu, S. M. Chen, Z. G. Zhao, C. Z. Lu, *Inorg. Chim. Acta* **2007**, *360*, 3484–3492; d) Y. Q. Lan, S. L. Li, K. Z. Shao, X. L. Wang, Z. M. Su, *Dalton Trans.* **2008**, 3824–3835; e) Y. Q. Lan, S. L. Li, X. L. Wang, K. Z. Shao, D. Y. Du, H. Y. Zang, Z. M. Su, *Inorg. Chem.* **2008**, *47*, 8179–8187.

[12] a) D. Hagrman, P. J. Hagrman, J. Zubieta, *Angew. Chem.* **1999**, *111*, 3359; *Angew. Chem. Int. Ed.* **1999**, *38*, 3165–3168; b) C. Inman, J. M. Knaust, S. W. Keller, *Chem. Commun.* **2002**, 156–157; c) X. L. Wang, Y. F. Bi, B. K. Chen, H. Y. Lin, G. C. Liu, *Inorg. Chem.* **2008**, *47*, 2442–2448; d) X. L. Wang, C. Qin, E. B. Wang, Z. M. Su, *Chem. Commun.* **2007**, 4245–4247; e) M. L. Wei, C. He, W. J. Hua, C. Y. Duan, S. H. Li, Q. J. Meng, *J. Am. Chem. Soc.* **2006**, *128*, 13318–13319; f) C. Y. Sun, S. X. Liu, D. D. Liang, K. Z. Shao, Y. H. Ren, Z. M. Su, *J. Am. Chem. Soc.* **2009**, *131*, 1883–1888; g) X. Y. Zhao, D. D. Liang, S. X. Liu, C. Y. Sun, R. G. Cao, C. Y. Gao, Y. H. Ren, Z. M. Su, *Inorg. Chem.* **2008**, *47*, 7133–7138.

[13] a) C. H. Li, K. L. Huang, Y. N. Chi, X. Liu, Z. G. Han, L. Shen, C. W. Hu, *Inorg. Chem.* **2009**, *48*, 2010–2017; b) X. Y. Liu, Y. Y. Jia, Y. F. Zhang, R. D. Huang, *Eur. J. Inorg. Chem.* **2010**, 4027–4033; c) Y. Z. Gao, Y. Q. Xu, Z. G. Han, C. H. Li, F. Y. Cui, Y. N. Chi, C. W. Hu, *J. Solid State Chem.* **2010**, *183*, 1000–1006.

[14] a) N. Sabbatini, M. Guardigi, F. Bolletta, I. Manet, R. Ziessel, *Angew. Chem. Int. Ed. Engl.* **1994**, *33*,1501–1503; b) X. P. Yang, R. A. Jones, *J. Am. Chem. Soc.* **2005**, *127*, 7686–7687; c) J. Xia, B. Zhao, H. S. Wang, W. Shi, Y. Ma, H. B. Song, P. Cheng, D. Z. Liao, S. P. Yan, *Inorg. Chem.* **2007**, *46*, 3450–3458.

[15] a) X. Y. Chen, B. Zhao, W. Shi, J. Xia, P. Cheng, D. Z. Liao, S. P. Yan, Z. H. Jiang, *Chem. Mater.* **2005**, *17*, 2866–2874; b) T. L. Daniel, S. G. Noel, L. C. Christopher, *Inorg. Chem.* **2005**, *44*, 258–266; c) V. Pavel, C. Peter, K. Jan, R. Jakub, H. Peter, L. Ivan, *Inorg. Chem.* **2005**, *44*, 5591–5599; d) T. M. Reineke, M. Eddaoudi, M. O'Keeffe, O. M. Yaghi, *Angew. Chem.* **1999**, *111*, 2712; *Angew. Chem. Int. Ed.* **1999**, *38*, 2590–2594; e) T. M. Reineke, M. Eddaoudi, M. Fehr, D. Kelley, O. M. Yaghi, *J. Am. Chem. Soc.* **1999**, *121*, 1651–1657; f) M. Eddaoudi, J. Kim, J. B. Wachter, H. K. Chae, M. O'Keeffe, O. M. Yaghi, *J. Am. Chem. Soc.* **2001**, *123*, 4368–4369; g) L. Pan, E. B. Woodlock, X. Wang, *Inorg. Chem.* **2000**, *39*, 4174–4178; h) R. Cao, D. F. Sun, Y. C. Liang, M. C. Hong, K. Tataumi, Q. Shi, *Inorg. Chem.* **2002**, *41*, 2087–2094; i) F. A. A. Paz, J. Klinowski, *Chem. Commun.* **2003**, 1484–1485; j) J. P. Costes, J. M. C. Juan, F. Dahan, F. Nicodème, *Dalton Trans.* **2003**, 1272–1275; k) M. Hernández-Molina, C. Ruiz-Pérez, T. López, F. Lloret, M. Julve, *Inorg. Chem.* **2003**, *42*, 5456–5458; l) X. J. Zheng, Z. M. Wang, S. Gao, F. H. Liao, C. H. Yan, L. P. Jin, *Eur. J. Inorg. Chem.* **2004**, 2968–2973.

[16] a) F. X. Geng, Y. Matsushita, R. Z. Ma, H. Xin, M. Tanaka, F. Izumi, N. Iyi, T. Sasaki, *J. Am. Chem. Soc.* **2008**, *130*, 16344–16350; b) X. Q. Zhao, B. Zhao, S. Wei, P. Cheng, *Inorg. Chem.* **2009**, *48*, 11048–11057; c) J. Xia, B. Zhao, H. S. Wang, W. Shi, Y. Ma, H. B. Song, P. Cheng, D. Z. Liao, S. P. Yan, *Inorg. Chem.* **2007**, *46*, 3450–3458; d) Y. G. Sun, X. F. Gu, F. Ding, P. F. Smet, E. J. Gao, D. Poelman, F. Verpoort, *Cryst. Growth Des.* **2010**, *10*, 1059–1067.

[17] a) J. C. Dai, X. T. Wu, Z. Y. Fu, C. P. Cui, S. M. Hu, W. X. Du, L. M. Wu, H. H. Zhang, R. Q. Sun, *Inorg. Chem.* **2002**, *41*, 1391–1396; b) S. Z. Li, P. T. Ma, J. P. Wang, Y. Y. Guo, H. Z. Niu, J. W. Zhao, J. Y. Niu, *CrystEngComm* **2010**, *12*, 1718–1721.

[18] a) G. E. Buono-Core, H. Li, *Coord. Chem. Rev.* **1990**, *99*, 55–87; b) M. Taki, H. Murakami, M. Sisido, *Chem. Commun.* **2000**, 1199–1200; c) M. Montalti, L. Prodi, N. Zaccheroni, L. Charbonniere, L. Douce, R. Ziessel, *J. Am. Chem. Soc.* **2001**, *123*, 12694–12695; d) Z. H. Zhang, T. A. Okamura, Y. Hasegawa, H. Kawaguchi, L. Y. Kong, W. Y. Sun, N. Ueyama, *Inorg. Chem.* **2005**, *44*, 6219–6227; e) Y. Li, F. K. Zheng, X. Liu, W. Q. Zou, G. C. Guo, C. Z. Lu, J. S. Huang, *Inorg. Chem.* **2006**, *45*, 6308–6316; f) J. W. Cheng, S. T. Zheng, E. Ma, G. Y. Yang, *Inorg. Chem.* **2007**, *46*, 10534–10538; g) E. G. Moore, J. Xu, C. J. Jocher, I. Castro-Rodriguez, K. N. Raymond, *Inorg. Chem.* **2008**, *47*, 3105–3118; h) Y. G. Huang, B. L. Wu, D. Q. Yuan, Y. Q. Xu, F. L. Jiang, M. C. Hong, *Inorg. Chem.* **2007**, *46*, 1171–1176; i) X. L. Wang, Y. Q. Guo, Y. G. Li, E. B. Wang, C. W. Hu, N. H. Hu, *Inorg. Chem.* **2003**, *42*, 4135–4140.

[19] a) D. R. Foster, F. S. Richardson, *Inorg. Chem.* **1983**, *22*, 3996–4002; b) S. Yanagida, Y. Hasegawa, K. Murakoshi, Y. Wada, N. Nakashima, T. Yamanaka, *Coord. Chem. Rev.* **1998**, *171*, 461–480; c) T. Yamada, S. Shinoda, H. Sugimoto, J. I. Uenishi, H. Tsukube, *Inorg. Chem.* **2003**, *42*, 7932–7937.

[20] a) P. Mialane, L. Lisnard, A. Mallard, J. Marrot, E. Antic-Fidancev, P. Aschehoug, D. Vivien, F. Sécheresse, *Inorg. Chem.* **2003**, *42*, 2102–2108; b) J. Y. Niu, K. H. Wang, H. N. Chen, J. W. Zhao, P. T. Ma, J. P. Wang, M. X. Li, Y. Bai, D. B. Dang, *Cryst. Growth Des.* **2009**, *9*, 4362–4372; c) J. C. G. Bünzli, C. Piguet, *Chem. Soc. Rev.* **2005**, *34*, 1048–1077; d) Y. Q. Sun, J. Zhang, Y. M. Chen, G. Y. Yang, *Angew. Chem.* **2005**, *117*, 5964; *Angew. Chem. Int. Ed.* **2005**, *44*, 5814–5817; e) Y. Q. Sun, J. Zhang, G. Y. Yang, *Chem. Commun.* **2006**, 1947–1949; f) Y. Q. Sun, J. Zhang, G. Y. Yang, *Chem. Commun.* **2006**, 4700–4702.

[21] a) G. M. Sheldrick, *SHELXL-97, Program for Crystal Structure Solution and Refinement*, version 5.1, University of Göttingen, Germany, **1997**; b) G. M. Sheldrick, *SADABS, Program for Empirical Absorption Correction of Area Detector Data*, University of Göttingen, Germany, **1996**.

Received: September 7, 2011
Published Online: November 9, 2011

